智能反射面辅助的环境反向散射通信系统信道估计算法研究

徐勇军* 邱友静 张海波
(重庆邮电大学通信与信息工程学院 重庆 400065)

摘 要：环境反向散射通信(AmBC)是一种新型的低功耗通信技术，它能利用周围环境中的射频(RF)信号源实现无源信息传输，但由于其存在双重衰落、障碍物阻挡等问题，导致反射链路信号强度弱。为此，该文将智能反射面(IRS)引入到AmBC系统中用以增强反射链路增益。然而，IRS与标签均为无源器件使得信道估计极具挑战性。为此，该文提出了一种IRS辅助的AmBC系统信道估计方案。首先，将信道分解为多个子信道，其中，反射链路的每个子信道对应一个IRS反射单元。然后，将最小二乘(LS)法作为估计准则，以最小化均方误差(MSE)为目标，探索了IRS反射模式与信道估计的联合设计。仿真结果表明，该信道估计方案具有良好的估计性能。

关键词：环境反向散射通信；智能反射面；信道估计
中图分类号：TN929.5 **文献标识码**：A **文章编号**：1009-5896(2025)01-0075-09
DOI: 10.11999/JEIT240395

1 引言

随着物联网(Internet of Things, IoT)在农业、工业、医疗等多个领域的广泛应用，人与设备，设备与设备之间的大量连接成为不可避免的趋势。然而，频谱稀缺、成本高昂以及能量限制严重阻碍了物联网的发展[1]。为此，作为新型无线传输技术的环境反向散射通信(Ambient Backscatter Communication, AmBC)[2]和智能反射面(Intelligent Reflective Surfaces, IRS)[3]受到了广泛关注。其中，AmBC通过利用周围环境中已有的射频(Radio Frequency, RF)信号(数字电视、蜂窝基站以及无线局域网)触发与阅读器的信息传递。相比于主动式通信设备，AmBC摆脱了电源的束缚以及对特定RF源的依赖，显著降低了功耗和成本。IRS作为一种低成本的无源结构，不同于传统的标签，其表面由大量可控的反射元件组成，可通过实时地操控相移器来配置无线传播环境，进而改善通信质量、扩大信号覆盖范围。由于在AmBC系统中，低功耗信号传输距离有限，容易受到障碍物遮挡导致信号衰减较大，将IRS应用到AmBC系统中可以有效地改善信号衰减问题，增强信号覆盖范围和传输距离，从而提升AmBC系统的性能[4]。

近年来，关于IRS辅助的AmBC系统的研究主要聚焦于性能分析[5]、波束赋形[6]、资源分配[7]，且大部分研究都假设系统的信道状态信息(Channel State Information, CSI)是完美已知的，然而在实际系统中，要获取精准的CSI具有一定的挑战性，故如何获取IRS辅助AmBC系统的CSI是一个亟待解决的关键科学问题。针对AmBC系统的信道估计问题，文献[8]采用期望最大化算法获取了带有单天线阅读器的AmBC系统中的信道模值。在此基础上，文献[9]考虑了多天线阅读器，并提出了一种基于协方差矩阵特征值分解的盲信道估计算法。进一步，文献[10]将信道拓展为频率选择性信道，以最小二乘(Least Squares, LS)法为准则结合迭代的思想，利用标签状态不同信道也不同的特点估计出了两路信道参数。文献[11]将AmBC系统中的信道估计建模为去噪问题，提出了一种基于卷积神经网络的深度残差学习去噪算法，并采用多个三维去噪模块提高了估计精度。考虑到硬件的不理想情况，文献[12]采用最大似然算法和期望最大化算法来联合估计信道参数、载波频偏以及同相/正交分量不平衡，证明了基于期望最大化算法的半盲估计器比基于最大似然算法的估计器精度及频带利用率更高但同时计算复杂度也更高。为了在两者之间寻求权衡，文献[13]考虑全双工多天线AmBC系统，提出了基于直接判决的半盲估计算法，该算法的估计精度与计算复杂度介于最大似然算法和期望最大法算法之间。考虑到标签内部能量收集模块具有严格的灵敏度约束，文献[14]研究了具有灵敏度约束的AmBC系统，引入最大似然估计器，提出了一种最小化信

收稿日期：2024-05-20；改回日期：2024-11-15；网络出版：2024-12-12
*通信作者： 徐勇军 xuyj@cqupt.edu.cn
基金项目：国家自然科学基金(62271094, U23A20279)，重庆市自然科学基金重点项目(CSTB2022NSCQ-LZX0009, CSTB2023NSCQ-LZX0079)，重庆市教委科技重点项目(KJZD-K202200601)
Foundation Items: The National Natural Science Foundation of China (62271094, U23A20279), The Key Fund of Natural Science Foundation of Chongqing (CSTB2022NSCQ-LZX0009, CSTB2023NSCQ-LZX0079), The Scientific and Technological Research Program of Chongqing Municipal Education Commission (KJZD-K202200601)

道估计均方误差的最优导频设计。在此基础上，文献[15]考虑了标签激活状态未知的情况，提出了基于信道概率密度函数的最大似然、线性最小均方误差和最大后验3种估计算法。

针对IRS辅助的单站式反向散射通信系统的信道估计问题，文献[16]采用LS算法获取了带有单天线标签和单天线阅读器的反向散射通信系统信道参数，并对IRS相移矩阵进行了优化使得信道估计误差最小，最终以封闭形式导出了最优解。由于单站式反向散射通信系统需要额外的RF源，这增加了部署的成本，且信号会产生往返路径损耗造成信号强度的大幅衰减，从而导致有效通信距离短[17]。因此，本文将更具有生态意义和一般性的AmBC系统与IRS技术相结合，研究了IRS辅助AmBC系统中的信道估计问题，主要贡献如下：

(1)与现有的AmBC系统信道估计研究不同[8–15]，本文考虑了标签和阅读器之间信号被建筑物阻挡的情况，为了增强反射链路增益，引入IRS，构建了IRS辅助的AmBC通用系统模型。

(2)单站式反向散射通信需要特定RF源且会产生往返路径损耗，存在局限性。不同于现有的IRS辅助的单站式反向散射通信系统信道估计研究[16]，本文考虑了AmBC系统，更契合低功耗、低成本的需求。

(3)根据所建立的模型，本文将信道分解为多个子信道，其中，反射链路的每个子信道对应一个IRS反射单元。并以LS算法为估计准则，探索了IRS反射模式与信道估计的联合设计。仿真验证了理论推导的正确性，分析了不同相移矩阵优化方法的估计性能，结果表明所提方案具有良好的估计性能且可以满足信道估计的精度要求。

本文符号说明：向量和矩阵分别用黑体小写字母和大写字母表示，$[\boldsymbol{A}]_{i,j}$表示矩阵$\boldsymbol{A}$的第i行j列个元素，$\boldsymbol{a}_i$表示向量$\boldsymbol{a}$的第i个元素，$\mathbb{C}$表示复数空间，$\mathbb{C}^{M\times N}$表示$M\times N$维的复数空间，$(\cdot)^{\mathrm{T}}$表示转置，$(\cdot)^{\mathrm{H}}$表示共轭转置，$(\cdot)^{-1}$表示逆运算，$|\cdot|$表示模运算，$||\cdot||_2$表示向量的2范数，$\mathrm{Tr}(\cdot)$表示矩阵的迹，$\mathrm{Rank}(\cdot)$表示矩阵的秩，$\mathrm{diag}(\cdot)$表示对角矩阵，$\mathbb{E}[\cdot]$表示随机变量的期望运算，$\boldsymbol{1}_N$表示N维全1列向量，$\boldsymbol{E}_N$表示$N\times N$维的全1矩阵。

2 系统模型

智能反射面辅助的AmBC系统如图1所示，包含4个组成部分：RF源、无源标签、IRS以及阅读器。其中，RF源、标签以及阅读器配置单根天线，IRS配置M个反射单元。此系统中，RF源传输信息给阅读器并向标签提供能量，同时，标签通过动态改变其电路阻抗将要传输的信息调制到RF信号上[18]。由于建筑物的遮挡，IRS用于辅助标签到阅读器之间的通信。最终，阅读器接收并解码来自RF源和经标签及IRS反射的两路信号。

定义$h\in\mathbb{C}$，$h_{\mathrm{t}}\in\mathbb{C}$，$\boldsymbol{f}\in\mathbb{C}^{1\times M}$，$\boldsymbol{g}\in\mathbb{C}^{M\times 1}$分别为RF源到阅读器，RF源到标签，标签到IRS，IRS到阅读器的信道增益，且所有信道均为平坦衰落信道。$\boldsymbol{\Phi}(n)=[\Phi_{n,1},\Phi_{n,2},\cdots,\Phi_{n,M}]^{\mathrm{T}}$为第$n$个时隙的IRS反射系数向量，其中，$\Phi_{n,m}=\beta_{n,m}\mathrm{e}^{\mathrm{j}\theta_{n,m}}$为第$n$个时隙第$m$个反射单元的反射系数，振幅$\beta_{n,m}\in[0,1]$，相移$\theta_{n,m}\in[0,2\pi]$。定义集合$\forall n,a\in\mathcal{N}=\{1,2,\cdots,N\},\forall m\in\mathcal{M}=\{1,2,\cdots,M\},\forall i,j,b\in\mathcal{M}_+=\{1,2,\cdots,M+1\}$。

假设在第n个时隙RF源发送的正交相移键控(Quadrature Phase Shift Keying, QPSK)信号为$x(n)$，阅读器能接收到来自RF源和经标签及IRS反射的两路信号。在此过程中，标签接收到的信号为

$$y_{\mathrm{t}}(n)=h_{\mathrm{t}}x(n) \tag{1}$$

然后，标签通过调节电路中的电阻，将要传输的二进制数据调制进RF信号中，具体来讲，标签可以通过反射或不反射RF信号两种状态传输0和1比特信息[19]。假设标签的二进制数据为$B(n)$，$B(n)\in\{0,1\}$，采用定时同步技术使信号$x(n)$和$B(n)$的到达时间同步[20]，此时阅读器接收的信号表示为

$$\begin{aligned}y(n)&=hx(n)+\eta y_{\mathrm{t}}(n)B(n)\boldsymbol{f}\mathrm{diag}\left(\boldsymbol{\Phi}(n)\right)\boldsymbol{g}+w(n)\\&=\left(h+\eta B(n)h_{\mathrm{t}}\boldsymbol{f}\mathrm{diag}\left(\boldsymbol{\Phi}(n)\right)\boldsymbol{g}\right)x(n)+w(n)\end{aligned} \tag{2}$$

其中，$\eta\in[0,1]$为标签的反射系数，$w(n)\sim\mathcal{CN}(0,\sigma^2)$为阅读器处均值为0，方差为$\sigma^2$的高斯白噪声。令$\boldsymbol{v}=h_{\mathrm{t}}\boldsymbol{f}\mathrm{diag}(\boldsymbol{g})=[v_1,v_2,\cdots,v_M]\in\mathbb{C}^{1\times M}$为通过标签和IRS的级联信道，故(2)式可写为

$$y(n)=\left(h+\eta B(n)\boldsymbol{v}\boldsymbol{\Phi}(n)\right)x(n)+w(n) \tag{3}$$

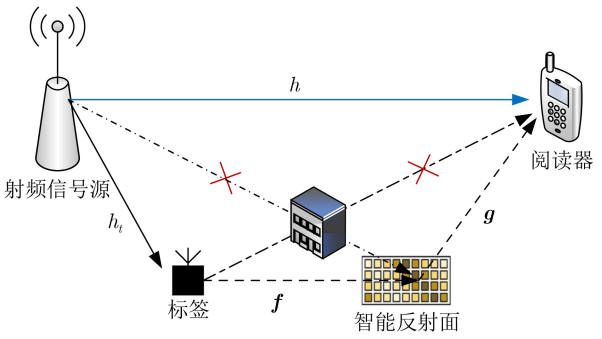

图 1 IRS辅助的AmBC系统

我们假设训练可以在相干时间内完成，这样，信道增益在训练期间保持不变[21]。设RF源发送N个导频符号$\boldsymbol{x}=[x(1),x(2),\cdots,x(N)]^{\mathrm{T}}$，在训练期间，标签呈全反射状态，即$B(n)=1$，$\eta=1$。阅读器接收到的信号表示为

$$\boldsymbol{y}=(h+\boldsymbol{v}\boldsymbol{\Phi})\boldsymbol{x}+\boldsymbol{w} \tag{4}$$

其中，$\boldsymbol{y}=[y(1),y(2),\cdots,y(N)]^{\mathrm{T}}$为接收信号向量，$\boldsymbol{\Phi}=[\Phi(1),\Phi(2),\cdots,\Phi(N)]^{\mathrm{T}}$为IRS反射矩阵，$\boldsymbol{w}=[w(1),w(2),\cdots,w(N)]^{\mathrm{T}}$为阅读器处的噪声，且$\boldsymbol{w}\sim\mathcal{CN}\cdot(0,\sigma^2\boldsymbol{I}_N)$。将式(4)改写为

$$\begin{bmatrix} y(1)\\ y(2)\\ \vdots\\ y(N)\end{bmatrix}=\begin{bmatrix} x(1)[1\ \Phi_{1,1}\ \cdots\ \Phi_{1,M}]\\ x(2)[1\ \Phi_{2,1}\ \cdots\ \Phi_{2,M}]\\ \vdots\\ x(N)[1\ \Phi_{N,1}\cdots\Phi_{N,M}]\end{bmatrix}\begin{bmatrix} h\\ v_1\\ \vdots\\ v_M\end{bmatrix}+\begin{bmatrix} w(1)\\ w(2)\\ \vdots\\ w(N)\end{bmatrix} \tag{5}$$

定义IRS相移矩阵为

$$\boldsymbol{\Theta}=\begin{bmatrix} 1 & \Phi_{1,1} & \cdots & \Phi_{1,M}\\ \vdots & \vdots & \ddots & \vdots\\ 1 & \Phi_{N,1} & \cdots & \Phi_{N,M}\end{bmatrix}\in\mathbb{C}^{N\times(M+1)} \tag{6}$$

令$\boldsymbol{\chi}=\mathrm{diag}(x(1),x(2),\cdots,x(N))$，$\boldsymbol{X}=\boldsymbol{\chi}\boldsymbol{\Theta}$，$\boldsymbol{\mu}=[h,v_1,\cdots,v_M]^{\mathrm{T}}$，则式(5)可改写为标准的线性形式

$$\boldsymbol{y}=\boldsymbol{X}\boldsymbol{\mu}+\boldsymbol{w} \tag{7}$$

3　信道估计

本小节研究了信道估计与IRS反射模式的联合设计，以LS法为估计准则，通过优化IRS相移矩阵$\boldsymbol{\Theta}$来最小化MSE。

3.1　基于LS的信道估计

假定$\boldsymbol{X}$满秩，根据LS估计器，我们可以得到信道参数$\boldsymbol{\mu}$的估计值[10]

$$\begin{aligned}\hat{\boldsymbol{\mu}}&=\arg\min\|\boldsymbol{y}-\boldsymbol{X}\boldsymbol{\mu}\|_2^2\\&=(\boldsymbol{X}^{\mathrm{H}}\boldsymbol{X})^{-1}\boldsymbol{X}^{\mathrm{H}}\boldsymbol{y}\\&=\boldsymbol{\mu}+\boldsymbol{\mu}_{\mathrm{e}}\end{aligned} \tag{8}$$

将式(7)代入式(8)，可以得到信道估计误差$\boldsymbol{\mu}_{\mathrm{e}}\triangleq(\boldsymbol{X}^{\mathrm{H}}\boldsymbol{X})^{-1}\boldsymbol{X}^{\mathrm{H}}\boldsymbol{w}$。故上述LS估计的MSE为

$$\begin{aligned}&\mathrm{MSE}(\hat{\boldsymbol{\mu}})\\&=\mathbb{E}\left[\|\boldsymbol{\mu}_{\mathrm{e}}\|_2^2\right]\\&=\mathbb{E}\left[\mathrm{Tr}\left((\boldsymbol{X}^{\mathrm{H}}\boldsymbol{X})^{-1}\boldsymbol{X}^{\mathrm{H}}\boldsymbol{w}\boldsymbol{w}^{\mathrm{H}}\boldsymbol{X}\left((\boldsymbol{X}^{\mathrm{H}}\boldsymbol{X})^{-1}\right)^{\mathrm{H}}\right)\right]\\&=\sigma^2\mathrm{Tr}\left((\boldsymbol{X}^{\mathrm{H}}\boldsymbol{X})^{-1}\right)\end{aligned} \tag{9}$$

由无偏估计理论可知，所要估计的矢量参数$\boldsymbol{\mu}$的克拉美罗界(Cramer-Rao Lower Bound, CRLB)会对每一个元素的方差设置一个下界[22]，即

$$\mathrm{var}\,(\hat{\boldsymbol{\mu}}_i)\geq\mathrm{CRLB}(\boldsymbol{\mu}_i)=\left[\boldsymbol{I}^{-1}(\boldsymbol{\mu})\right]_{i,i},\ \forall i \tag{10}$$

其中，$\boldsymbol{I}(\boldsymbol{\mu})$为Fisher信息矩阵，由式(11)给出

$$[\boldsymbol{I}(\boldsymbol{\mu})]_{i,j}=-E\left[\frac{\partial^2\ln p(\boldsymbol{y};\boldsymbol{\mu})}{\partial\boldsymbol{\mu}_i\partial\boldsymbol{\mu}_j}\right],\ \forall i,j \tag{11}$$

其中，$p(\boldsymbol{y};\boldsymbol{\mu})$为接收信号$\boldsymbol{y}$的概率密度函数，通过求2阶偏导和取均值得到Fisher信息$\boldsymbol{I}(\boldsymbol{\mu})$的最终表达式为

$$\boldsymbol{I}(\boldsymbol{\mu})=\frac{\boldsymbol{X}^{\mathrm{H}}\boldsymbol{X}}{\sigma^2} \tag{12}$$

因此，信道参数$\boldsymbol{\mu}_i$的CRLB为

$$\mathrm{CRLB}(\boldsymbol{\mu}_i)=\left[\sigma^2\left(\boldsymbol{X}^{\mathrm{H}}\boldsymbol{X}\right)^{-1}\right]_{i,i},\ \forall i \tag{13}$$

由于式(7)为高斯线性模型，故LS估计量是最小方差无偏(Minimum Variance Unbiased, MVU)估计量，且是有效的，它达到了CRLB，因此信道估计值$\hat{\boldsymbol{\mu}}$的协方差矩阵为[23]

$$\boldsymbol{C}_{\hat{\boldsymbol{\mu}}}=\boldsymbol{I}^{-1}(\boldsymbol{\mu})=\sigma^2(\boldsymbol{X}^{\mathrm{H}}\boldsymbol{X})^{-1} \tag{14}$$

结合式(9)，可以看出$\mathrm{MSE}(\hat{\boldsymbol{\mu}})=\mathrm{Tr}\,(\boldsymbol{C}_{\hat{\boldsymbol{\mu}}})=\mathrm{Tr}\left(\boldsymbol{I}^{-1}(\boldsymbol{\mu})\right)$，假设整个训练周期的功率分配是相等的且每个导频信号为单位功率信号，即$|x(n)|^2=1$，$\forall n$，故$\boldsymbol{\chi}^{\mathrm{H}}\boldsymbol{\chi}=\boldsymbol{I}_N$。此时估计参数$\hat{\boldsymbol{\mu}}$的MSE为

$$\begin{aligned}\mathrm{MSE}(\hat{\boldsymbol{\mu}})&=\sigma^2\mathrm{Tr}\left((\boldsymbol{X}^{\mathrm{H}}\boldsymbol{X})^{-1}\right)\\&=\sigma^2\mathrm{Tr}\left((\boldsymbol{\Theta}^{\mathrm{H}}\boldsymbol{\chi}^{\mathrm{H}}\boldsymbol{\chi}\boldsymbol{\Theta})^{-1}\right)\\&=\sigma^2\mathrm{Tr}\left((\boldsymbol{\Theta}^{\mathrm{H}}\boldsymbol{\Theta})^{-1}\right)\end{aligned} \tag{15}$$

3.2　IRS相移矩阵设计

在本节中，我们的目标是通过优化IRS相移矩阵$\boldsymbol{\Theta}$来最小化式(15)中的MSE。优化问题可以表示为

$$\begin{aligned}\mathrm{P1}:\ &\min_{\boldsymbol{\Theta}}\ \sigma^2\mathrm{Tr}\left((\boldsymbol{\Theta}^{\mathrm{H}}\boldsymbol{\Theta})^{-1}\right)\\&\text{s.t. }\mathrm{C}_1:[\boldsymbol{\Theta}]_{a,1}=1,\ \forall a\\&\qquad\mathrm{C}_2:0\leq\beta_{n,m}\leq1,\ \forall n,m\\&\qquad\mathrm{C}_3:0\leq\theta_{n,m}\leq2\pi,\ \forall n,m\\&\qquad\mathrm{C}_4:\mathrm{Rank}(\boldsymbol{\Theta})=M+1\end{aligned} \tag{16}$$

其中，C_1表示相移矩阵的第1列元素取1用以估计直连信道h，C_2为IRS反射单元的反射幅度约束，C_3为IRS反射单元的相移约束，C_4为相移矩阵$\boldsymbol{\Theta}$的满秩约束。

首先采用ON/OFF法[24]来估计$M+1$个信道参数，假设$N=M+1$。在N个导频时隙，标签始终保持反射状态，在第1个时隙，IRS关闭所有的反射单

元来估计RF源到阅读器的直连信道。在其他时隙，IRS通过逐个打开反射单元来分别估计级联信道。通过将IRS振幅和相移系数设置为$\beta_{n,m}=1$，$\theta_{n,m}=0$和$\beta_{n,m}=0$来实现反射单元的开闭，即

$$[\boldsymbol{\Theta}]_{a,b}=\begin{cases}1, & (a=1)\vee(a=b)\\ 0, & (a\neq 1)\wedge(a\neq b)\end{cases},\ \forall a,b \tag{17}$$

将式(17)代入式(15)，可求得信道估计参数$\hat{\boldsymbol{\mu}}$的MSE

$$\begin{aligned}\mathrm{MSE}(\hat{\boldsymbol{\mu}})&=\sigma^2\mathrm{Tr}\left(\left(\boldsymbol{\Theta}^{\mathrm{H}}\boldsymbol{\Theta}\right)^{-1}\right)\\&=\sigma^2\mathrm{Tr}\begin{pmatrix}1 & -\boldsymbol{1}_M^{\mathrm{T}}\\ -\boldsymbol{1}_M & \boldsymbol{E}_M+\boldsymbol{I}_M\end{pmatrix}\end{aligned} \tag{18}$$

此外，可得出直连信道估计参数$\hat{h}$的MSE为

$$\mathrm{MSE}(\hat{h})=\sigma^2 \tag{19}$$

级联信道估计参数$\hat{\boldsymbol{v}}_m$的MSE为

$$\mathrm{MSE}(\hat{\boldsymbol{v}}_m)=2\sigma^2,\ \forall m \tag{20}$$

由此可见，ON/OFF法级联信道的MSE为直连信道MSE的两倍，这是由于在级联信道估计阶段，每个时隙只有一个IRS反射元件打开将导频信号反射至阅读器处进行估计，且直连信道的估计误差会叠加到级联信道的估计中，因此信道估计的精度较低。

虽然采用ON/OFF法来优化相移矩阵可以满足式(16)中的约束条件，但不是P1的最优解。为了进一步降低MSE，我们结合Fisher信息矩阵的性质[21]，即

$$\left[\boldsymbol{I}^{-1}(\boldsymbol{\mu})\right]_{i,i}\geq\frac{1}{[\boldsymbol{I}(\boldsymbol{\mu})]_{i,i}},\ \forall i \tag{21}$$

当且仅当Fisher信息矩阵$\boldsymbol{I}(\boldsymbol{\mu})$为对角矩阵时等号成立。由于$\mathrm{MSE}(\hat{\boldsymbol{\mu}})=\mathrm{Tr}\left(\boldsymbol{I}^{-1}(\boldsymbol{\mu})\right)$，根据式(15)可知当$\boldsymbol{\Theta}^{\mathrm{H}}\boldsymbol{\Theta}$为对角矩阵时，可以取到$\mathrm{MSE}(\hat{\boldsymbol{\mu}})$的下界。假设存在这样可行的设计，因此我们可以等价地最大化$\mathrm{Tr}(\boldsymbol{\Theta}^{\mathrm{H}}\boldsymbol{\Theta})$，此时**P1**转化为

$$\begin{aligned}\mathrm{P2}:\ &\max_{\boldsymbol{\Theta}}\ \mathrm{Tr}(\boldsymbol{\Theta}^{\mathrm{H}}\boldsymbol{\Theta})\\&\text{s.t. }\mathrm{C}_1-\mathrm{C}_4\\&\quad\mathrm{C}_5:\boldsymbol{\Theta}^{\mathrm{H}}\boldsymbol{\Theta}=\mathrm{diag}(\alpha_1,\alpha_2,\cdots,\alpha_{M+1})\end{aligned} \tag{22}$$

为了求解P2，采用基于DFT矩阵的方法构造$\boldsymbol{\Theta}$[25]。定义一个$N\times N$维的DFT矩阵$\boldsymbol{W}_N$

$$\boldsymbol{W}_N=\begin{bmatrix}1 & 1 & \cdots & 1\\ 1 & \mathrm{e}^{-\mathrm{j}2\pi/N} & \cdots & \mathrm{e}^{-\mathrm{j}2(N-1)\pi/N}\\ \vdots & \vdots & \ddots & \vdots\\ 1 & \mathrm{e}^{-\mathrm{j}2(N-1)\pi/N} & \cdots & \mathrm{e}^{-\mathrm{j}2(N-1)(N-1)\pi/N}\end{bmatrix} \tag{23}$$

故$\boldsymbol{W}_N^{\mathrm{H}}\boldsymbol{W}_N=\boldsymbol{W}_N\boldsymbol{W}_N^{\mathrm{H}}=N\boldsymbol{I}_N$，取DFT矩阵$\boldsymbol{W}_N$的前$N$行，$M+1$列构成相移矩阵$\boldsymbol{\Theta}$，其中$N\geq M+1$，故

$$[\boldsymbol{\Theta}]_{a,b}=[\boldsymbol{W}_{N,M+1}^{\mathrm{H}}]_{a,b}=\mathrm{e}^{-\mathrm{j}2\pi(a-1)(b-1)/N},\ \forall a,b \tag{24}$$

可以推导出

$$\boldsymbol{\Theta}^{\mathrm{H}}\boldsymbol{\Theta}=\boldsymbol{W}_{N,M+1}^{\mathrm{H}}\boldsymbol{W}_{N,M+1}=N\boldsymbol{I}_{M+1} \tag{25}$$

由此可见，$\boldsymbol{\Theta}$的设计满足P2中的约束条件。进一步证明该设计是最优的，因为P2的目标有如式(26)所示上界

$$\mathrm{Tr}(\boldsymbol{\Theta}^{\mathrm{H}}\boldsymbol{\Theta})=\sum_{a=1}^{N}\sum_{b=1}^{M+1}\left|[\boldsymbol{\Theta}]_{a,b}\right|^2\leq N(M+1) \tag{26}$$

由式(25)可知，显然，$\boldsymbol{\Theta}$的设计达到了式(26)的上界，即

$$\mathrm{Tr}(\boldsymbol{\Theta}^{\mathrm{H}}\boldsymbol{\Theta})=\mathrm{Tr}(\boldsymbol{W}_{N,M+1}^{\mathrm{H}}\boldsymbol{W}_{N,M+1})=N(M+1) \tag{27}$$

故$\boldsymbol{\Theta}=\boldsymbol{W}_{N,M+1}$是P2的最优解。

同样，也可以采用基于Hadamard矩阵的方法来构造$\boldsymbol{\Theta}$[26]。定义一个$N\times N$维的Hadamard矩阵$\boldsymbol{H}_N$如下

$$\left.\begin{aligned}\boldsymbol{H}_N=\boldsymbol{H}_{2^\lambda}&=\begin{bmatrix}\boldsymbol{H}_{2^{\lambda-1}} & \boldsymbol{H}_{2^{\lambda-1}}\\ \boldsymbol{H}_{2^{\lambda-1}} & -\boldsymbol{H}_{2^{\lambda-1}}\end{bmatrix}\\ \boldsymbol{H}_2&=\begin{bmatrix}1 & 1\\ 1 & -1\end{bmatrix}\end{aligned}\right\} \tag{28}$$

其中，$N=2^\lambda$，$\lambda>0$为正整数。故$\boldsymbol{H}_N^{\mathrm{H}}\boldsymbol{H}_N=\boldsymbol{H}_N\boldsymbol{H}_N^{\mathrm{H}}=N\boldsymbol{I}_N$，取Hadamard矩阵$\boldsymbol{H}_N$的前$N$行，$M+1$列即$\boldsymbol{H}_{N,M+1}$构成$\boldsymbol{\Theta}$，故

$$\boldsymbol{\Theta}^{\mathrm{H}}\boldsymbol{\Theta}=\boldsymbol{H}_{N,M+1}^{\mathrm{H}}\boldsymbol{H}_{N,M+1}=N\boldsymbol{I}_{M+1} \tag{29}$$

不难证明$\boldsymbol{\Theta}$的设计同样满足P2中的约束条件且是最优的。与基于DFT矩阵构造$\boldsymbol{\Theta}$不同的是，基于Hadamard矩阵构造的$\boldsymbol{\Theta}$仅有两个离散的相移值，即$\theta_{n,m}=0$或$\theta_{n,m}=\pi$，进一步降低了IRS硬件的实施复杂性。

基于上述两种方法，可以得到LS信道估计参数$\hat{\mu}$的MSE为

$$\begin{aligned}\mathrm{MSE}(\hat{\boldsymbol{\mu}})&=\sigma^2\mathrm{Tr}\left(\left(\boldsymbol{W}_{N,M+1}^{\mathrm{H}}\boldsymbol{W}_{N,M+1}\right)^{-1}\right)\\&=\sigma^2\mathrm{Tr}\left(\left(\boldsymbol{H}_{N,M+1}^{\mathrm{H}}\boldsymbol{H}_{N,M+1}\right)^{-1}\right)\\&=\sigma^2\mathrm{Tr}\left(N\boldsymbol{I}_{M+1}\right)\\&=\sigma^2\frac{M+1}{N}\end{aligned} \tag{30}$$

其中，直连及级联信道估计参数的MSE为

$$\mathrm{MSE}(\hat{h})=\mathrm{MSE}(\hat{\boldsymbol{v}}_m)=\frac{\sigma^2}{N},\ \forall m \tag{31}$$

4 仿真结果与分析

本节通过Matlab仿真来验证算法的有效性。在

仿真中，信道建模为瑞利衰落信道，噪声服从0均值的高斯分布，导频信号$x(n)$为QPSK信号且$|x(n)|^2=1$，设置发射天线和接收天线的数量为1，标签反射系数$\eta=1$。所有仿真结果是取1 000次蒙特卡罗实验的平均值[25]，估计器的性能由MSE以及CRLB来衡量。

图2–图3显示了不同算法下直连信道及级联信道MSE随信噪比的变化，同时绘制出了不同算法下估计参数的CRLB。在仿真中，设置反射单元数$M=19$，导频数量$N=M+1=20$，以满足式(16)的约束，信噪比SNR$\in[-5\text{ dB},40\text{ dB}]$。CRLB展示了最优无偏估计的方差，为估计算法提供了下限。由图可见，3种算法的MSE与其CRLB拟合，与理论分析一致，说明算法达到了最佳的性能。同时，3种算法的MSE随着信噪比的增大而减小，这是由于在高信噪比条件下，信号所受的噪声干扰较小，接收到的信号质量更高，这意味着观测数据的质量更高，更高质量的观测数据有助于提高信道估计的准确性，从而降低了估计参数的MSE。此外，基于DFT方法的MSE与基于Hadamard方法的MSE相同，相较于ON/OFF法，基于DFT和Hadamard方法的MSE更小，且直连信道与级联信道的MSE相等，而ON/OFF法级联信道的MSE为直连信道MSE的两倍，这是由于ON/OFF法直连信道的估计误差会传递到级联信道的估计中。

图4–图5显示了不同算法在不同信噪比下直连信道及级联信道MSE随IRS反射单元数量的变化。在仿真中，设置反射单元数量$M\in[3,127]$，导频数量$N=M+1$，信噪比为20dB和40dB。由图可见，随着IRS反射单元数量的增加，基于ON/OFF法的MSE保持不变，而基于DFT和Hadamard方法的MSE减小。其次，3种方法在高信噪比下MSE均低于在低信噪比下的MSE。这是由于ON/OFF法的MSE与IRS反射单元数量无关，仅与噪声方差有关，

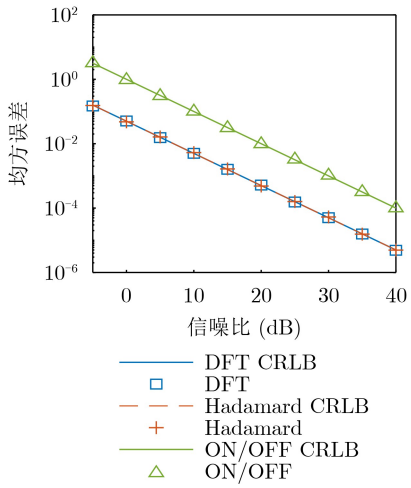

图 2 直连信道均方误差随信噪比变化曲线

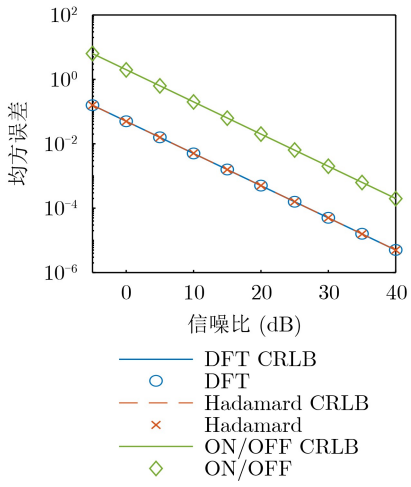

图 3 级联信道均方误差随信噪比变化曲线

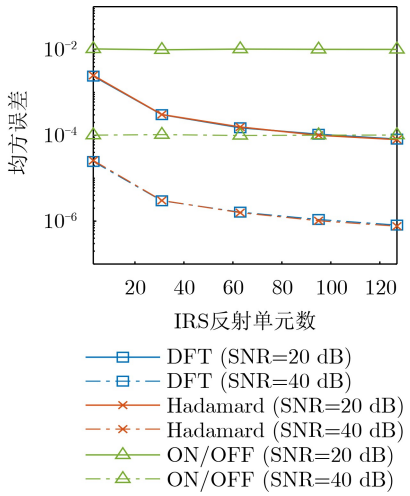

图 4 直连信道均方误差随反射单元数变化曲线

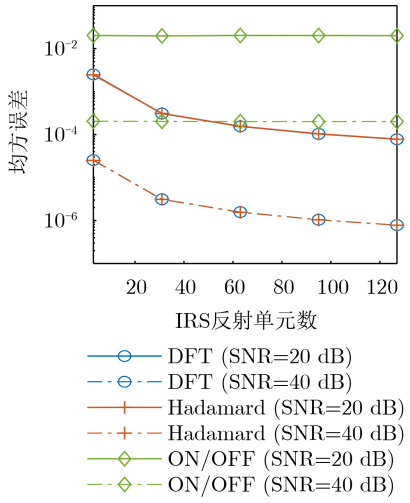

图 5 级联信道均方误差随反射单元数变化曲线

而基于DFT和Hadamard方法的MSE不光与噪声方差有关还与IRS反射单元数有关，由于M作为N的函数，IRS反射单元数量的增加意味着需要更多的导频，而更多的导频有助于更准确地估计信道，从而减少估计误差。由此说明了基于DFT和Hadamard的方法估计性能更好且更适用于大规模IRS。

图6–图7显示了不同算法在不同信噪比下直连信道及级联信道MSE随导频数量的变化。在仿真中，设置导频数量$N \geq M+1$，其中IRS反射单元数量$M=15$固定不变，$N \in [16, 128]$，信噪比分别为20 dB和40 dB。由图可见，随着导频数量的增加，基于DFT和Hadamard方法的MSE减小。这是由于导频信号本质上是用于估计信道特性的观测量，增加导频数量会增加观测到的信号数量，从而提供更多的信息用于估计，使估计结果更加准确。由此说明了虽然增加导频数量会占用额外的信道带宽并产生更多的功率开销，但它可以有效地降低MSE从而提高估计精度。

5 结论

为了解决IRS辅助的AmBC系统信道估计问题，本文提出了一种以LS为准则的信道估计算法。通过将信道分解为多个子信道进行估计来获取所需的CSI。同时采用ON/OFF法、基于DFT矩阵和Hadamard矩阵构建IRS相移矩阵来最小化MSE。仿真结果验证了该信道估计方案具有良好的估计性能。

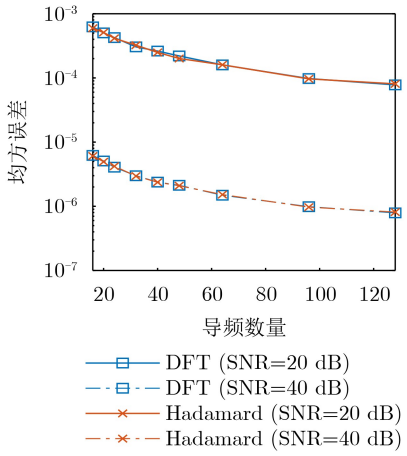

图 6 直连信道均方误差随反射单元数变化曲线

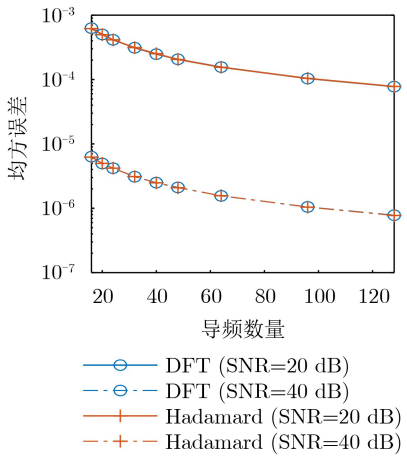

图 7 级联信道均方误差随反射单元数变化曲线

参 考 文 献

[1] XU Yongjun, GUI Guan, GACANIN H, *et al*. A survey on resource allocation for 5G heterogeneous networks: Current research, future trends, and challenges[J]. *IEEE Communications Surveys & Tutorials*, 2021, 23(2): 668–695. doi: 10.1109/COMST.2021.3059896.

[2] 张晓茜, 徐勇军. 面向零功耗物联网的反向散射通信综述[J]. 通信学报, 2022, 43(11): 199–212. doi: 10.11959/j.issn.1000-436x.2022199.

ZHANG Xiaoxi and XU Yongjun. Survey on backscatter communication for zero-power IoT[J]. *Journal on Communications*, 2022, 43(11): 199–212. doi: 10.11959/j.issn.1000-436x.2022199.

[3] XU Yongjun, XIE Hao, WU Qingqing, *et al*. Robust max-min energy efficiency for RIS-aided HetNets with distortion noises[J]. *IEEE Transactions on Communications*, 2022, 70(2): 1457–1471. doi: 10.1109/TCOMM.2022.3141798.

[4] GALAPPATHTHIGE D L, REZAEI F, TELLAMBURA C, *et al*. RIS-empowered ambient backscatter communication systems[J]. *IEEE Wireless Communications Letters*, 2023, 12(1): 173–177. doi: 10.1109/LWC.2022.3220158.

[5] LE A T, NGUYEN T N, TU L T, *et al*. Performance analysis of RIS-assisted ambient backscatter communication systems[J]. *IEEE Wireless Communications Letters*, 2024, 13(3): 791–795. doi: 10.1109/LWC.2023.3344113.

[6] 张晓茜, 徐勇军, 吴翠先, 等. 智能反射面增强的全双工环境反向散射通信系统波束成形算法[J]. 电子与信息学报, 2024, 46(3): 914–924. doi: 10.11999/JEIT230356.

ZHANG Xiaoxi, XU Yongjun, WU Cuixian, *et al*. Beamforming design for reconfigurable intelligent surface enhanced full-duplex ambient backscatter communication networks[J]. *Journal of Electronics & Information Technology*, 2024, 46(3): 914–924. doi: 10.11999/JEIT230356.

[7] YANG Hancheng, DING Haiyang, CAO Kunrui, *et al*. A RIS-segmented symbiotic ambient backscatter communication system[J]. *IEEE Transactions on Vehicular Technology*, 2024, 73(1): 812–825. doi: 10.1109/TVT.2023.3306037.

[8] MA Shuo, WANG Gongpu, FAN Rongfei, *et al*. Blind channel estimation for ambient backscatter communication systems[J]. *IEEE Communications Letters*, 2018, 22(6): 1296–1299. doi: 10.1109/LCOMM.2018.2817555.

[9] ZHAO Wenjing, WANG Gongpu, ATAPATTU S, *et al*.

Blind channel estimation in ambient backscatter communication systems with multiple-antenna reader[C]. Proceedings of 2018 IEEE/CIC International Conference on Communications in China, Beijing, China, 2018: 320–324. doi: 10.1109/ICCChina.2018.8641171.

[10] ZHU Yue, WANG Gongpu, TANG Hengliang, *et al*. Channel estimation for ambient backscatter systems over frequency-selective channels[C]. Proceedings of 2018 IEEE/CIC International Conference on Communications in China, Beijing, China, 2018: 384–388. doi: 10.1109/ICCChina.2018.8641250.

[11] LIU Xuemeng, LIU Chang, LI Yonghui, *et al*. Deep residual learning-assisted channel estimation in ambient backscatter communications[J]. *IEEE Wireless Communications Letters*, 2021, 10(2): 339–343. doi: 10.1109/LWC.2020.3030222.

[12] ABDALLAH S, SALAMEH A I, and SAAD M. Joint channel, carrier frequency offset and I/Q imbalance estimation in ambient backscatter communication systems[J]. *IEEE Communications Letters*, 2021, 25(7): 2250–2254. doi: 10.1109/LCOMM.2021.3075493.

[13] ABDALLAH S, VERBOVEN Z, SAAD M, *et al*. Channel estimation for full-duplex multi-antenna ambient backscatter communication systems[J]. *IEEE Transactions on Communications*, 2023, 71(5): 3059–3072. doi: 10.1109/TCOMM.2023.3251387.

[14] CUI Ziqi, WANG Gongpu, WEI Xusheng, *et al*. Channel estimation and optimal training design for ambient backscatter communication systems under sensitivity constraint[C]. Proceedings of 2022 IEEE 96th Vehicular Technology Conference, London, United Kingdom, 2022: 1–5. doi: 10.1109/VTC2022-Fall57202.2022.10012695.

[15] CUI Ziqi, WANG Gongpu, GAO Jie, *et al*. Channel estimation for backscatter communication systems under circuit sensitivity constraint[J]. *IEEE Transactions on Vehicular Technology*, 2024, 73(5): 7441–7446. doi: 10.1109/TVT.2023.3347926.

[16] ABEYWICKRAMA S, YOU Changsheng, ZHANG Rui, *et al*. Channel estimation for intelligent reflecting surface assisted backscatter communication[J]. *IEEE Wireless Communications Letters*, 2021, 10(11): 2519–2523. doi: 10.1109/LWC.2021.3106165.

[17] LIN Junliang, WANG Gongpu, XU Rongtao, *et al*. Versatile-modulation and megabit-rate backscatter system: Design, implementation, and experimental results[J]. *IEEE Internet of Things Journal*, 2024, 11(5): 8240–8252. doi: 10.1109/JIOT.2023.3318634.

[18] LI Dong. Two birds with one stone: Exploiting decode-and-forward relaying for opportunistic ambient backscattering[J]. *IEEE Transactions on Communications*, 2020, 68(3): 1405–1416. doi: 10.1109/TCOMM.2019.2957490.

[19] XU Yongjun, GU Bowen, HU R Q, *et al*. Joint computation offloading and radio resource allocation in MEC-based wireless-powered backscatter communication networks[J]. *IEEE Transactions on Vehicular Technology*, 2021, 70(6): 6200–6205. doi: 10.1109/TVT.2021.3077094.

[20] D'AMICO A A and MORELLI M. Symbol-spaced feedforward techniques for blind bit synchronization and channel estimation in FSO-OOK communications[J]. *IEEE Transactions on Communications*, 2024, 72(1): 361–374. doi: 10.1109/TCOMM.2023.3317931.

[21] GU Bowen, LI Dong, LIU Ye, *et al*. Exploiting constructive interference for backscatter communication systems[J]. *IEEE Transactions on Communications*, 2023, 71(7): 4344–4359. doi: 10.1109/TCOMM.2023.3277519.

[22] XIE Ning, XU Yuntao, ZHANG Jiaheng, *et al*. Joint estimation of channel responses and phase noises in asynchronous MIMO systems with intentional timing offset[J]. *IEEE Transactions on Communications*, 2023, 71(1): 412–426. doi: 10.1109/TCOMM.2022.3223711.

[23] SENGIJPTA S K. Fundamentals of statistical signal processing: Estimation theory[J]. *Technometrics*, 1995, 37(4): 465–466. doi: 10.1080/00401706.1995.10484391.

[24] MISHRA D and JOHANSSON H. Channel estimation and low-complexity beamforming design for passive intelligent surface assisted MISO wireless energy transfer[C]. Proceedings of 2019 IEEE International Conference on Acoustics, Speech and Signal Processing, Brighton, United Kingdom, 2019: 4659–4663. doi: 10.1109/ICASSP.2019.8683663.

[25] JENSEN T L and DE CARVALHO E. An optimal channel estimation scheme for intelligent reflecting surfaces based on a minimum variance unbiased estimator[C]. Proceedings of 2020 IEEE International Conference on Acoustics, Speech and Signal Processing, Barcelona, Spain, 2020: 5000–5004. doi: 10.1109/ICASSP40776.2020.9053695.

[26] ZHOU Zhengyi, GE Ning, WANG Zhaocheng, *et al*. Joint transmit precoding and reconfigurable intelligent surface phase adjustment: A decomposition-aided channel estimation approach[J]. *IEEE Transactions on Communications*, 2021, 69(2): 1228–1243. doi: 10.1109/TCOMM.2020.3034259.

徐勇军：男，教授，博士生导师，研究方向为反向散射通信、智能反射面、信道估计、资源分配等.

邱友静：女，硕士生，研究方向为反向散射通信、智能反射面、信道估计等.

张海波：男，副教授，硕士生导师，研究方向为资源分配、反向散射通信、车联网等.

责任编辑：陈　倩

Channel Estimation for Intelligent Reflecting Surface Assisted Ambient Backscatter Communication Systems

XU Yongjun QIU Youjing ZHANG Haibo

(*School of Communication and Information Engineering, Chongqing University of Posts and Telecommunications, Chongqing* 400065, *China*)

Abstract:

Objective Ambient Backscatter Communication (AmBC) is an emerging, low-power, low-cost communication technology that utilizes ambient Radio Frequency (RF) signals for passive information transmission. It has demonstrated significant potential for various wireless applications. However, in AmBC systems, the reflected signals are often severely weakened due to double fading effects and signal obstruction from environmental obstacles. This results in a substantial reduction in signal strength, limiting both communication range and overall system performance. To address these challenges, Intelligent Reflecting Surface (IRS) technology has been integrated into AmBC systems. IRS can enhance reflection link gain by precisely controlling reflected signals, thereby improving system performance. However, the passive nature of both the IRS and tags makes accurate channel estimation a critical challenge. This study proposes an efficient channel estimation algorithm for IRS-assisted AmBC systems, aiming to provide theoretical support for optimizing system performance and explore the feasibility of achieving high-precision channel estimation in complex environments—key to the practical implementation of this technology.

Methods This study develops a general IRS-assisted AmBC system model, where the system channel is divided into multiple subchannels, each corresponding to a specific IRS reflection element. To minimize the Mean Squared Error (MSE) in channel estimation, the Least Squares (LS) method is used as the estimation criterion. The joint optimization problem for channel estimation is explored by integrating various IRS reflection modes, including ON/OFF, Discrete Fourier Transform (DFT), and Hadamard modes. The communication channel is assumed to follow a Rayleigh fading distribution, with noise modeled as zero-mean Gaussian. Pilot signals are modulated using Quadrature Phase Shift Keying (QPSK). To thoroughly evaluate the performance of channel estimation, 1000 Monte Carlo simulations are conducted, with MSE and the Cramer-Rao Lower Bound (CRLB) serving as performance metrics. Simulation experiments conducted on the Matlab platform provide a comprehensive comparison and analysis of the performance of different algorithms, ultimately validating the effectiveness and accuracy of the proposed algorithm.

Results and Discussions The simulation results demonstrate that the IRS-assisted channel estimation algorithm significantly improves performance. Under varying Signal-to-Noise Ratio (SNR) conditions, the MSE of methods based on DFT and Hadamard matrices consistently outperforms the ON/OFF method, aligning with the CRLB, thereby confirming the optimal performance of the proposed algorithms (Fig. 2, Fig. 3). Additionally, the MSE for direct and cascaded channels is identical when using the DFT and Hadamard methods, while the cascaded channel MSE for the ON/OFF method is twice that of the direct channel, highlighting the superior performance of the DFT and Hadamard approaches. As the number of IRS reflection elements increases, the MSE for the DFT and Hadamard methods decreases significantly, whereas the MSE for the ON/OFF method remains unchanged (Fig. 4, Fig. 5). This illustrates the ability of the DFT and Hadamard methods to effectively exploit the scalability of IRS, demonstrating better adaptability and estimation performance in large-scale IRS systems. Furthermore, increasing the number of pilot signals leads to a further reduction in MSE for the DFT and Hadamard methods, as more pilot signals provide higher-quality observations, thereby enhancing channel estimation accuracy (Fig. 6, Fig. 7). Although additional pilot signals consume more resources, their substantial impact on reducing MSE highlights their importance in improving estimation precision. Moreover, under high-SNR conditions, the MSE for all algorithms is lower than that under low-SNR conditions, with the DFT and Hadamard methods showing more pronounced reductions (Fig. 4, Fig. 5).

This indicates that the proposed methods enable more efficient channel estimation under better signal quality, further enhancing system performance. In conclusion, the channel estimation algorithms based on DFT and Hadamard matrices offer significant advantages in large-scale IRS systems and high-SNR scenarios, providing robust support for optimizing low-power, low-cost communication systems.

Conclusions This paper presents a low-complexity channel estimation algorithm for IRS-assisted AmBC systems based on the LS criterion. The channel is decomposed into multiple subchannels, and the optimization of IRS phase shifts is designed to significantly enhance both channel estimation and transmission performance. Simulation results demonstrate that the proposed algorithm, utilizing the DFT and Hadamard matrices, achieves excellent performance across various SNR and system scale conditions. Specifically, the algorithm effectively reduces the MSE of channel estimation, exhibits higher estimation accuracy under high-SNR conditions, and shows low computational complexity and strong robustness in large-scale IRS systems. These results provide valuable insights for the theoretical modeling and practical application of IRS-assisted AmBC systems. The findings are particularly relevant for the development of low-power, large-scale communication systems, offering guidance on the design and optimization of IRS-assisted AmBC systems. Additionally, this work lays a solid theoretical foundation for the advancement of next-generation Internet of Things applications, with potential implications for future research on IRS technology and their integration with AmBC systems.

Key words: Ambient Backscatter Communication (AmBC); Intelligent Reflecting Surface (IRS); Channel estimation